Single-Channel Imaging at Low Sampling Rates

Salah Skitioui, Cyril Decroze, Ettien Kpré, Christophe Gaguière, Okan Yurduseven, and Thomas Fromentèze

***Abstract*—This study introduces a method for single-channel imaging at low sampling rates, utilizing Frequency-Modulated Continuous Wave radar combined with space-frequency multiplexing. This approach significantly reduces system complexity and data acquisition demands by encoding scene reflectivity into a single, low-frequency signal. A mathematical framework supporting this technique is developed and followed by an experimental demonstration, where an image is reconstructed using a transmit antenna and a 15-element receive array within the 92–96 GHz band, whose interaction is converted into a single beat signal with a 32 MHz bandwidth.**

***Index Terms*—Radar Imaging, Computational imaging, Frequency modulation, Computational electromagnetics.**

I. Introduction

THE extension of computational imaging to the microwave and millimeter-wave ranges has underscored the potential for reducing the number of active channels in imaging systems [1], [2], [3], [4], [5]. This emerging field requires the development of apertures capable of radiating signals independent in both space and frequency. When combined with the resolution of inverse problems, this approach enables three-dimensional image reconstruction from the encoding of scene reflectivity into a reduced set of measurements [6], [7], [8]. This paper leverages this concept within Frequency-Modulated Continuous Wave (FMCW) based architectures, which are prevalently used in radar and imaging systems [9], [10]. By mixing a reference signal with its delayed, scene-interacted counterpart, one obtains beat signals of significantly lower frequencies [11]. Adapting these transceiver architectures to computational imaging, we propose to limit the complexity of the associate systems to a potential single active chain whose sampling frequency can now be limited to a few megahertz. Following the development of suitable reconstruction formalisms in this paper, an experimental validation of the principle is presented.

II. FMCW computational imaging

A. Space-frequency multiplexing in the physical layer

In this work, a frequency-diverse antenna is integrated with an FMCW transceiver, aiming to simultaneously reduce the redundancy of active chains in imaging systems and their sampling frequencies (Fig.1). The principle of computational imaging lies in the development of antennas capable of emitting spatial field distributions that are weakly correlated, varying with the operating frequency [1], [2] or the polarization of lumped elements [12]. Adopting a model simplified using the first Born approximation, the measured samples correspond to a linear combination of the reflectivity of a scene to be imaged $\sigma(r)$, through a sensing matrix that represents the product of transmitted and received fields, $E_T(r,f)$ and $E_R(r,f)$ [13].

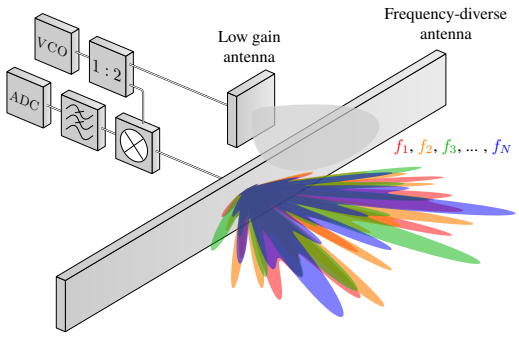

Fig. 1. Computational FMCW imaging system. The combination of a frequency-diverse antenna and an FMCW architecture enables both limiting the number of active channels and alleviating frequency sampling constraints for imaging. VCO and ADC mean respectively Voltage Controlled Oscillator and Analog-to-Digital Converter.

A frequency measurement using the generic system introduced in Fig. 1 then takes the following form, focusing for now only on the interaction between the antennas according to a scalar model:

$$S(f) = \int_r E_T(r,f)\ \sigma(r)\ E_R(r,f)\,\mathrm{d}r \tag{1}$$

$$= \int_r \Psi(r_T,r,f)\ \sigma(r)\ \sum_i M_i(f)\,\Psi(r_{R_i},r,f)\,\mathrm{d}r. \tag{2}$$

Following the system depiction provided in Fig. 1, in (1) and (2), the transmit antenna is the low gain antenna whereas the frequency-diverse antenna is the receiver. The radiation of the low-gain antenna is simplified here by the free-space Green's function Ψ, also used to describe the receive field of the frequency-diverse antenna, consisting of a sum of radiating elements with positions r_{R_i} and transfer functions $M_i(f)$ to the measurement port [14]. As introduced in [1], the radiation of spatially uncorrelated field distributions can be realized by means of pseudo-orthogonal $M_i(f)$ transfer functions, notably achievable with the frequency selectivity of highly multimodal cavities [6]. In many previous works, the efficiency of this computational imaging technique has been demonstrated by achieving an estimation of the reflectivity such that $\hat{\boldsymbol{\sigma}} = (\mathbf{E}_T \cdot \mathbf{E}_R)^{+}\mathbf{s}$. Here, $.^{+}$ stands for the pseudo-inverse of the sensing matrix of the system [6]. Measuring the frequency signal $\mathbf{s}$, represented as a vector, remains a

S. Skitioui, C. Decroze and T. Fromentèze are with the University of Limoges, XLIM, UMR 7252, F-87000 Limoges, France

Ettien Kpré is with Thalès Defense & Security Elancourt, France

C. Gaquière is with the Université Polytechnique Hauts de France, UMR 8520—Institut d'Electronique de Microélectronique et de Nanotechnologie (IEMN), Université de Lille, F-59000 Lille, France

O. Yurduseven is with the Centre for Wireless Innovation (CWI), School of Electronics, Electrical Engineering and Computer Science (EEECS), Queen's University Belfast, BT3 9DT Belfast, U.K

major constraint for frequency-diverse computational imaging systems given that it occupies wide and densely sampled frequency bandwidths (typically on the order of several GHz).

B. Adaptation to FMCW systems and forward modeling

By combining an FMCW architecture with a frequency-diverse antenna, the measured frequency signal is converted into a baseband time signal consisting of a multitude of beat frequencies down to a few MHz. It is then necessary to develop mathematical formalisms adapted to this setup, facilitating the reconstruction of spatial information from a low-frequency beat signal $b(t)$, defined as:

$$b(t) = \Re(F_{LP}\big(c(t)^* \cdot (c(t) * s(t))\big), \tag{3}$$

where $s(t) = \mathfrak{F}^{-1}\big(S(f)\big)$ is the inverse Fourier transform of $S(f)$, $*$ stands for the convolution product, $\Re()$ the real part of a complex signal, F_{LP} is the function of a low-pass filter, and where $c(t)$ is a signal linearly modulated in frequency, also defined as a chirp using the complex notation :

$$c(t) = \exp\big(j\,2\pi f_t(t)\,t + \epsilon(t)\big). \tag{4}$$

A triangular modulation is employed, for which the formalisms are defined for an upward slope. The instantaneous frequency $f_t(t)$ thus takes the form $f_t(t) = f_{\text{min}} + \frac{1}{2}\,\alpha\,t$. In this expression, f_{min} corresponds to the minimum operating frequency, $\alpha = B/T$ is the frequency sweep rate, where B is the bandwidth and T is the duration of each linear modulation. The term $\epsilon(t)$ accounts for potential non-linearity effects causing a deviation from the expected linear variation of instantaneous frequency. The latter will be disregarded for lightening the notations, but its detrimental effect must be considered during the experimental validation.

The formalism is now developed for a single isotropic scatterer set in the region of interest. It will then be possible to generalize it to a more complex scene using the superposition principle for a series of elements of index p, with reflectivity defined as $\sigma(r) = \delta(r - r_p)$, where r_p is the position of each scatterer.

Considering the previous free-space Green's function model, the receive signal can then be decomposed as follows in the time domain:

$$s(t) = \sum_p s_p(t) = \sum_p A_{p_i}\delta(t - \tau_{p_i}), \tag{5}$$

where $\tau_{p_i} = (|r_T - r_p|)/c + (|r_p - r_R|)/c$ corresponds to the delay induced by the elementary scatterer p as seen by each transceiver pair, decomposing the frequency-diverse aperture into a set of elementary radiating elements. The magnitude term derived from the product of the free space Green's functions is $A_{p_i} = 1/(16\pi^2|r_T - r_p||r_p - r_{R_i}|)$. This model ignores the effects of bandwidth limits to simplify the next steps, considering that the latter will be included by convolution with the input signal. Before being mixed with the reference modulated signal, the expression results in:

$$c(t) * s_p(t) = \sum_i c(t) * m_i(t) * A_{p_i}\,\delta(t - \tau_{p_i}), \tag{6}$$

To establish an analytical expression of the beat signal, we first aim to highlight that $\mathfrak{F}^{-1}\big(C(f)\,M_i(f)\big) = c(t) * m_i(t)$ is analogous to computing the Fourier transform of the impulse responses of the frequency-diverse sub-elements:

$$c(t) * m_i(t) = \int_\tau c(\tau)\,m_i(-(\tau - t))\,d\tau \tag{7}$$

$$= \int_\tau \exp\left(j2\pi f_t(\tau)\cdot\tau\right) m_i(-(\tau - t))\,d\tau. \tag{8}$$

To this end, the duration of the chirp T should be several order of magnitude greater than the time spread of the impulse responses $m_i(t)$. As depicted in Fig. 2, this convolution can be expressed as a Fourier transform:

$$c(t) * m_i(t) \approx \int_\tau \exp\left(j\,2\pi f_t(t)\cdot\tau\right) m_i(-(\tau - t))\,d\tau \tag{9}$$

$$\approx M_i\big(f_t(t)\big)\exp\left(j2\pi f_t(t)\cdot t\right). \tag{10}$$

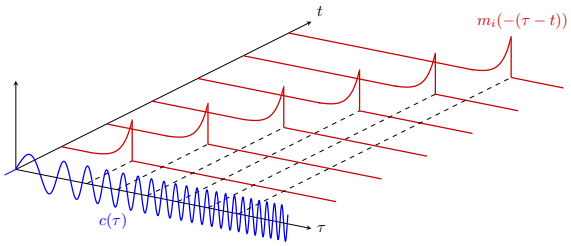

Fig. 2. Convolution of a chirp $c(t)$ (blue) with an impulse response $m_i(t)$ (depicted in the figure through its envelope) of a radiating element composing the frequency-diverse aperture (red). The delay spread of $m_i(t)$ is sufficiently short compared to the duration of the chirp so that a harmonic with constant frequency is locally considered.

The negative sign associated with the time-reversed impulse responses $m_i(-\tau)$ is compensated for by the absence of a minus sign in the definition of the Fourier transform. Consequently, the time signal received by the frequency-diverse antenna can be expressed as follows:

$$c(t) * s_p(t) = \sum_i c(t) * m_i(t) * A_{p_i}\,\delta(t - \tau_{p_i}) \tag{11}$$

$$\approx \sum_i A_{p_i}\left(M_i(f_t(t))\exp(j\,2\pi f_t(t)\cdot t)\right) * \delta(t - \tau_{p_i}) \tag{12}$$

$$\approx \sum_i A_{p_i}\,M_i\big(f_t(t - \tau_{p_i})\big)\,\exp\left(j2\pi f_t(t - \tau_{p_i})\cdot(t - \tau_{p_i})\right). \tag{13}$$

The signal received before mixing thus corresponds to a superposition of the time-shifted chirp signal modulated by the time delayed transfer functions (Fig. 3).

Multiplying by the modulated reference signal finally yields the expression of the beat signal $b_p(t)$ in response of a single isotropic scatterer of index p:

$$b_p(t) = \sum_i A_{p_i}\,M_i\big(f_t(t - \tau_{p_i})\big)\,\exp\left(j\phi(t)\right), \tag{14}$$

where $\phi(t) = 2\pi(-(f_{\text{min}} + \alpha t)\tau_{p_i} + \frac{1}{2}\alpha\tau_{p_i}^2)$ corresponds to the remaining phase terms after simplification, identical to those obtained with conventional FMCW systems [15].

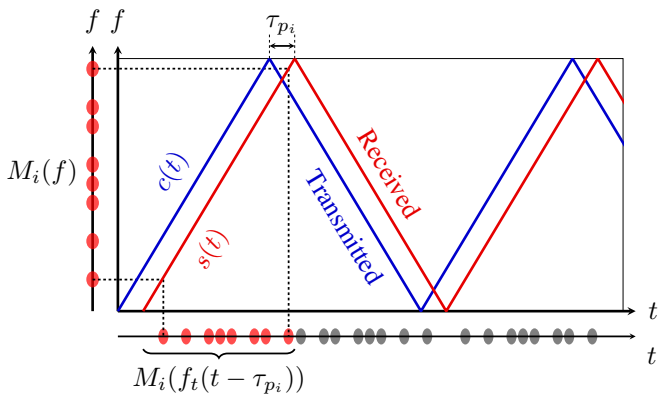

Fig. 3. Effect of frequency modulation on the conversion of frequency-diverse antenna transfer functions into time responses enabling multiplexing of radiating aperture signals, then converted into low-frequency beat signals.

A point scatterer finally corresponds to a sum of time-domain transposed and delayed transfer functions of the frequency-diverse antenna, to which deterministic phase terms are applied that can be compensated for when solving the associated inverse problem. Considering now that a target consists of a superposition of scatterers whose spatial reflectivity is defined by $\sigma(r_p)$, a measurement finally adopts the following form:

$$b(t) = \sum_{r_p} b_p(t)\,\sigma(r_p). \tag{15}$$

A series of simplifications are considered. The quadratic phase term $\pi\alpha\tau_{p_i}^2$, also defined as the residual video phase, can be disregarded for near-field applications involving short propagation delays. In other cases, it is possible to correct this phase using an appropriate filter [15], [16]. As discussed in a following section, the effect of delays applied to the time-domain transposed transfer functions $M_i\big(f_t(t-\tau_{p_i})\big) \approx M_i\big(f_t(t)\big)$ can be neglected for short-range operation. The expression of the beat signal is simplified as follows:

$$b(t) \approx \sum_{r_p}\sum_{i} M_i\big(f_t(t)\big)\,G_i(r_p)\,\sigma(r_p), \tag{16}$$

where $G_i(r_p) = A_{p_i}\,\exp\big(-j\,2\pi(f_{\min}+\alpha t)\,\tau_{p_i}\big)$ represents the product of free space Green's functions.

C. Solving the associated inverse problem

Following the derivation of the mathematical formalisms for the forward model, the associated inverse problem can now be solved. To this end, leveraging common computational imaging-based algorithms, two reconstruction methods can be employed [14]. The simplest and most straightforward is to define a linear operator encompassing both the transfer functions of the frequency-diversity antenna and Green's functions:

$$b(t) \approx \sum_{r_p} H(t, r_p)\,\sigma(r_p), \tag{17}$$

with $H(t, r_p) = \sum_i M_i\big(f_t(t)\big)\,G_i(r_p)$. Following a vectorization of the data, the estimate then takes the form:

$$\hat{\boldsymbol{\sigma}} = \mathbf{H}^{+}\mathbf{b}, \tag{18}$$

recalling that $.^{+}$ corresponds to a pseudo-inversion.

The reconstruction can be accelerated by performing this procedure in two steps, first estimating the signals received by the frequency-diverse antenna by equalizing its transfer functions, and then compensating the Green's functions:

$$\hat{\boldsymbol{\sigma}} = \mathbf{G}^{+}(\mathbf{M}^{+} \odot \mathbf{B}). \tag{19}$$

The symbol $\odot$ stands for the element-wise multiplication and the matrix $\mathbf{B}$ corresponds to a concatenation of identical vectors $\mathbf{b}$ until reaching the dimensions of $\mathbf{M}^{+}$.

In line with previous studies, the first method tends to offer the best estimates, but the second speeds up computations by reducing the volume of data to be processed in the back-propagation and even allows the $\mathbf{G}^{+}$ operator to be replaced by faster reconstruction techniques in the Fourier domain [14], [17]. Before presenting an experimental validation of these reconstructions, we identify the parameters influencing the sampling frequency required for the proper operation of an FMCW computational imaging system.

D. Sampling constraints and validity of the approximations

The efficiency of a frequency-diverse antenna in computational imaging is linked to its composite quality factor (or Q-factor), which reflects the ability to radiate uncorrelated field distributions between two sufficiently distant operating frequencies [6]. Considering that its impulse responses follow a magnitude decay law of $\exp(-t/(2\tau))$, this quality factor is defined as $Q = 2\pi f_c \tau$ [18], [19]. This time constant directly defines the temporal spread of signals at the output of the receiving antenna, neglecting the minor impact of propagation delays. Considering that the time responses are damped after 7τ (i.e. 3% of the initial amplitude [18]), the highest beat frequency $f_b^{\max}$ is then:

$$f_b^{\max} \approx 7\tau\frac{B}{T} = 7\frac{Q}{2\pi f_c}\frac{B}{T}. \tag{20}$$

The sampling frequency of this single receiver therefore depends on the combination of 4 parameters. While the quality factor, center frequency and operating band are generally imposed by the needs of the imaging activity, the duration T of the frequency-modulated signal represents a simple and direct means of transposing signals to just a few MHz (or even kHz) of bandwidth.

These data also play a central role in the previous approximations. The proper operation of this system relies on the frequency selectivity of the reception antenna. The quality factor also takes the form $Q = 2\pi f_c/\delta_f$, where δ_f corresponds to the average spectral distance between independent modes of its transfer functions $M_i(f)$. The validity of the approximation presented in Eq. (16) therefore depends on $|f_t(t-\tau_{p_i}) - f_t(t)| < \delta_f$ to ensure the correct compensation of the transfer functions. Consequently, the approximation is valid if the propagation delays respect $\tau_{p_i} < 4\pi T f_c/(BQ)$.

III. Experimental demonstration

A validation of this new technique is proposed in the 92–96 GHz band, exploiting the radiating component developed

for a previous demonstration using a vector network analyzer [20]. The frequency-modulated signal, generated within the frequency band of 11.5–12 GHz and with a duration of 32 μs, is produced by an Analog Devices ADF4159 demo board. This signal is then up-converted by a multiplier and amplified within the 92–96 GHz band. The transmit antenna is a low gain, open-ended WR-10 waveguide. The receive antenna is a leaky cavity with a composite quality factor of 23,000, defined from a decay time $\tau = 39$ ns. A series of 15 slots is arranged on the front panel, forming an array of radiating elements covering an extension of 57 mm, for an element spacing of approximately $1.3\,\lambda$ at the center frequency (Fig. 4). The distance between the center of the array and the transmit antenna is 8 cm. The receiving chain incorporates a low-noise amplifier, a mixer, and a low-pass filter. The transmit and receive chains were conceived and fabricated by MC2-Technologies. The targets are metal rods with a length of 30 cm and a diameter of 1.3 cm, positioned at a distance of 50 cm from the imaging system (Fig. 5). The measurement of the transfer functions is performed by positioning the transmit antenna in front of each slot of the cavity (Fig. 4). This technique is considered for the integration and compensation of the nonlinearities $\epsilon(t)$ distorting the signals $M_i\big(f_t(t)\big)$ and impacting the subsequent estimations.

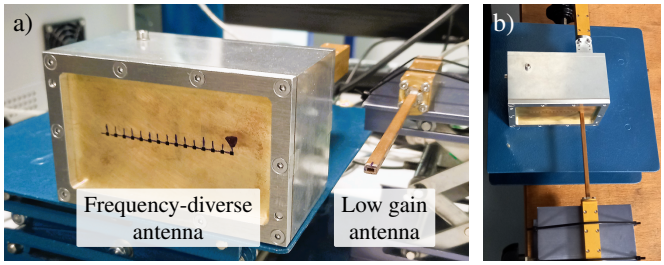

Fig. 4. Experimental imaging setup with receive and transmit antennas b) Measurement of the transfer functions $M_i(f_t(t))$.

In connection with the previous developments, the highest beat frequency of this system is estimated at only $f_b^{\max} = 32$ MHz. The approximation presented in Eq. (16) is valid as long as the propagation delays τ_{p_i} remain below 410 ns considering the data of this system, which is a round-trip propagation distance of less than 60 m.

A demonstration is performed with a sampling frequency of 72 MHz, tolerating a weak aliasing. Following the measurement of echoes from three metallic cylinders, the unique beat signal measured on the reception chain allows for the computation of images presented in Fig. 5 with a cross-range resolution of 2.4 cm and a range resolution of 4.4 cm. A reconstruction is carried out with the sensing matrix $\mathbf{H}$ in Eq. (18) in 5 ms, while the approach based on intermediate equalization, associated with Eq. (19), is performed in 0.8 ms.

For both images, the pseudo-inverses are computed by truncated singular value decomposition and stored in memory. A factor 6 acceleration in computation time is achieved at the cost of a slight degradation in image quality. Although in both cases the metrics obtained remain compatible with real-time

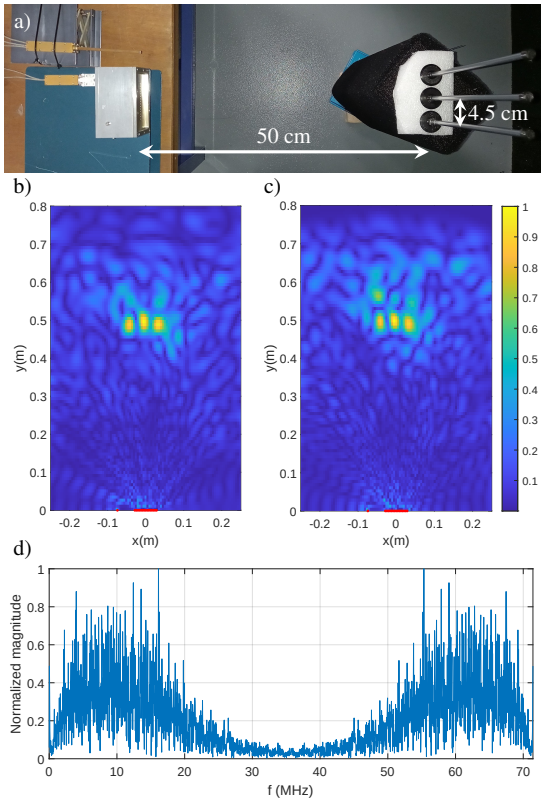

Fig. 5. Experimental validation: a) Imaging setup, b) Estimation with the full $\mathbf{H}$-matrix, c) Estimation by equalization, d) Spectrum of the single-channel beat signal $b(t)$ sampled at 72 MHz, used for image computation.

operations, the equalization offers a useful optimization for the development of larger imaging systems [17].

IV. Conclusion

This study successfully demonstrates a novel single-channel imaging technique utilizing FMCW radar and space-frequency multiplexing, now operating at low sampling rates.

By encoding scene reflectivity into a single, low-frequency signal, we significantly reduced the complexity and data acquisition demands of conventional computational imaging systems. The developed mathematical framework and the experimental validation, featuring a transmit antenna and a 15-element frequency-diverse receive array operating within the 92–96 GHz band, underscore the method's efficacy. The resulting single beat signal with a 32 MHz bandwidth proves the potential of this approach for efficient, high-resolution imaging across various applications.

Following on from the hardware simplifications offered by the development of computational imaging in the radio frequency bands, this new approach provides a solution to the constraints associated with sampling speed, which seemed to represent the last obstacle to the development of streamlined imaging systems.

V. Acknowledgment

This research benefited from the support of the Platinom platform, with funding from Nouvelle Aquitaine council and the European Union under the PILIM program.

REFERENCES

[1] D. Carsenat and C. Decroze, "Uwb antennas beamforming using passive time-reversal device," *IEEE Antennas and Wireless Propagation Letters*, vol. 11, pp. 779–782, 2012.

[2] J. Hunt, T. Driscoll, A. Mrozack, G. Lipworth, M. Reynolds, D. Brady, and D. R. Smith, "Metamaterial apertures for computational imaging," *Science*, vol. 339, no. 6117, pp. 310–313, 2013.

[3] M. Zhao, S. Zhu, H. Huang, D. Hu, X. Chen, J. Chen, and A. Zhang, "Frequency–polarization sensitive metasurface antenna for coincidence imaging," *IEEE Antennas and Wireless Propagation Letters*, vol. 20, no. 7, pp. 1274–1278, 2021.

[4] C. Saigre-Tardif, R. Faqiri, H. Zhao, L. Li, and P. del Hougne, "Intelligent meta-imagers: from compressed to learned sensing," *Applied Physics Reviews*, vol. 9, no. 1, 2022.

[5] R. Obermeier and J. A. Martinez-Lorenzo, "Sensing matrix design via mutual coherence minimization for electromagnetic compressive imaging applications," *IEEE Transactions on Computational Imaging*, vol. 3, no. 2, pp. 217–229, 2017.

[6] T. Fromenteze, O. Yurduseven, M. F. Imani, J. Gollub, C. Decroze, D. Carsenat, and D. R. Smith, "Computational imaging using a mode-mixing cavity at microwave frequencies," *Applied Physics Letters*, vol. 106, no. 19, 2015.

[7] M. Zhao, S. Zhu, X. Chen, T. Fromenteze, Q. H. Abbasi, A. Alomainy, V. Fusco, and O. Yurduseven, "Three-dimensional computational polarimetric imaging with a hyperuniform frequency-diverse metacavity transceiver," *IEEE Transactions on Instrumentation and Measurement*, 2024.

[8] M. F. Imani, J. N. Gollub, O. Yurduseven, A. V. Diebold, M. Boyarsky, T. Fromenteze, L. Pulido-Mancera, T. Sleasman, and D. R. Smith, "Review of metasurface antennas for computational microwave imaging," *IEEE transactions on antennas and propagation*, vol. 68, no. 3, pp. 1860–1875, 2020.

[9] K. B. Cooper, R. J. Dengler, N. Llombart, B. Thomas, G. Chattopadhyay, and P. H. Siegel, "Thz imaging radar for standoff personnel screening," *IEEE Transactions on terahertz science and technology*, vol. 1, no. 1, pp. 169–182, 2011.

[10] M. Alizadeh, G. Shaker, J. C. M. De Almeida, P. P. Morita, and S. Safavi-Naeini, "Remote monitoring of human vital signs using mm-wave fmcw radar," *IEEE Access*, vol. 7, pp. 54 958–54 968, 2019.

[11] G. Mathers, "Homodyne generator and detection system," in *WESCON/57 Conference Record*, vol. 1. IEEE, 1957, pp. 194–200.

[12] T. A. Sleasman, M. F. Imani, A. V. Diebold, M. Boyarsky, K. P. Trofatter, and D. R. Smith, "Implementation and characterization of a two-dimensional printed circuit dynamic metasurface aperture for computational microwave imaging," *IEEE Transactions on Antennas and Propagation*, vol. 69, no. 4, pp. 2151–2164, 2020.

[13] G. Lipworth, A. Rose, O. Yurduseven, V. R. Gowda, M. F. Imani, H. Odabasi, P. Trofatter, J. Gollub, and D. R. Smith, "Comprehensive simulation platform for a metamaterial imaging system," *Applied optics*, vol. 54, no. 31, pp. 9343–9353, 2015.

[14] T. Fromenteze, E. L. Kpré, C. Decroze, D. Carsenat, O. Yurduseven, M. Imani, J. Gollub, and D. R. Smith, "Unification of compressed imaging techniques in the microwave range and deconvolution strategy," in *2015 European Radar Conference (EuRAD)*. IEEE, 2015, pp. 161–164.

[15] A. Meta, P. Hoogeboom, and L. P. Ligthart, "Signal processing for fmcw sar," *IEEE Transactions on geoscience and remote sensing*, vol. 45, no. 11, pp. 3519–3532, 2007.

[16] F. Berland, H. H. Elwan, D. Boudescoque, C. Decroze, P. Di Bin, C. Aupetit-Berthelemot, and T. Fromenteze, "Solving the phase dispersion issue in fmcw photonic time multiplexed radar imaging," in *2021 15th European Conference on Antennas and Propagation (EuCAP)*. IEEE, 2021, pp. 1–5.

[17] T. Fromenteze, E. L. Kpré, D. Carsenat, C. Decroze, and T. Sakamoto, "Single-shot compressive multiple-inputs multiple-outputs radar imaging using a two-port passive device," *IEEE Access*, vol. 4, pp. 1050–1060, 2016.

[18] D. A. Hill, *Electromagnetic fields in cavities: deterministic and statistical theories*. John Wiley & Sons, 2009.

[19] D. L. Marks, J. Gollub, and D. R. Smith, "Spatially resolving antenna arrays using frequency diversity," *JOSA A*, vol. 33, no. 5, pp. 899–912, 2016.

[20] S. Skitioui, T. Fromentèze, E. Kpré, C. Gaquière, and C. Decroze, "Study of analog multiplexing techniques applied to millimeter wave imaging," in *Passive and Active Millimeter-Wave Imaging XXV*, vol. 12111. SPIE, 2022, pp. 114–123.